RSC Advances

PAPER

View Article Online
View Journal | View Issue

Cite this: *RSC Adv.*, 2022, **12**, 23704

A comparative study of the mechanical stability, electronic, optical and photocatalytic properties of $CsPbX_3$ (X = Cl, Br, I) by DFT calculations for optoelectronic applications

M. Aktary, * M. Kamruzzaman and R. Afrose

Organic free Cs-based perovskite materials are potential candidates for electronic and optoelectronic applications. A systematic comparative study of the mechanical, electronic, optical, and photocatalytic properties of $CsPbX_3$ (X = Cl, Br, I) was conducted using density functional theory to compare the applicability of these materials in optoelectronic, photocatalytic, and photovoltaic (PV) devices. We calculated structural and elastic properties to determine the better agreement of damage-tolerance and electronic and optical responses for suitable device applications. Optimized lattice parameters and elastic constants showed excellent agreement with the experimental data whereas some properties were found to be much better than other theoretical reports. $CsPbBr_3$ is thermodynamically more stable and more ductile compared to the other two perovskites. The hydrostatic pressure dependent mechanical stability showed that $CsPbCl_3$ and $CsPbBr_3$ sustained stability under low applied pressure, whereas the stability of $CsPbI_3$ was very high. The electronic band gap calculations showed that $CsPbCl_3$, $CsPbBr_3$, and $CsPbI_3$ are suitable for green, orange, and red emissions of optical spectra owing to the proper electronic band gaps. $CsPbI_3$ can be shown as the best photocatalyst for the hydrogen evolution reaction and $CsPbBr_3$ is the most stable photocatalyst due to its nearly balanced oxidation and reduction potentials, but $CaPbCl_3$ is better for O_2 production. The density of states and other optical properties have been reported in this study. Thus, our findings would be beneficial for experimental studies and can open a new window for efficient electronic, optoelectronic, and hydrogen production along with the biodegradation of polluted and waste materials.

Received 23rd July 2022
Accepted 5th August 2022

DOI: 10.1039/d2ra04591e

rsc.li/rsc-advances

1. Introduction

The demand for more efficient PV cells, optoelectronic and electronic devices is of great concern with the increasing world population under the worse conditions of insufficient energy crisis.[1] With this increasing demand, researchers are extremely careful on a healthy ecosystem. A new kind of effective, eco-friendly, and renewable energy capturing technology has achieved much more interest among the world scientific community.[2–11] The present photovoltaic market is dominated by Si-based solar cells[12,13] but they do not work for long due to low efficiency and maintenance of the expensive purification processes.[1] Besides, their less optical absorption, less carrier mobility, and indirect band type[1] have made this rethinkable in the competitive race for the production of more functioning device, and the amorphous Si thin film technology is cost-effective and the fabrication process is simple. However, its low stability as well as lower photo conversion efficiency (PCE) are of great concern.[14,15] Thus, researchers are eagerly concerned to find alternative low-cost, earth-abundant, and solution-processable solar cell materials. To this end, organic–inorganic halide perovskites meet these demands and are of great interest. In the 1990s, perovskite materials started their research journey extensively for the replacement of Si and multifunctional solar cell devices.

The perovskite solar cell was first reported by Miyasaka and co-workers in 2006 and they reported a PCE of ~2.2%[16,17] that reached 3.8% in 2009.[18] In 2018, a research report on a PCE of 27.6% was published, which mentioned that a 30% plus PCE was possible by the end of 2020, but in 2020, the US National Renewable Energy Laboratory certified a perovskite solar cell with a max. PCE of 25.5%.[19] Researchers found hope for mixed halide perovskites from a comparative study of different structures. Thus organic–inorganic lead halide perovskites solar cells have drawn incredible attention in the scientific community as alternative competitors to some inorganic photovoltaic materials, such as copper indium gallium sulfide and selenide (CIGS), cadmium telluride (CdTe), amorphous or single crystal silicon (a-Si or c-Si), iron disulphide (FeS_2), and gallium

Department of Physics, Begum Rokeya University, Rangpur, Rangpur-5400, Bangladesh. E-mail: aktarymahbuba@gmail.com; Tel: (+88) 01516795931

arsenide (GaAs). Though multi-junction AlGaInP, AlGaAs, GaAs, GaInAs cells are certified as 47.1% efficient in the present research,[20] all of these compounds are expensive due to the presence of scarcity elements, In, and Ga, and they are also toxic as they contain As and P. Hence, metal halide perovskites[21–31] solar cells have a great possibility to replace the dominating Si-based solar cells by proper selection of atoms in a right place. Organic–inorganic halide perovskites with a formula of AMX_3 (where, organic–inorganic cation A = $CH_3NH_3^+$ or Cs^+, *etc.*; inorganic cation M = Pb^{2+} or Sn^{2+}, *etc.*; halide X = Cl^-, Br^-, I^-)[1,32] are highly[33–36] efficient due to excellent absorption coefficient,[37–39] carrier mobility, lengthy carrier life, and a suitable band gap.[40–45] Due to low physical and chemical stabilities of organic–inorganic perovskites,[1] inorganic perovskites have achieved tremendous research interest. Among them, Cs-based inorganic perovskites $CsPbX_3$ (X = Cl, Br, I) are promising materials for next-generation advanced electronic, optoelectronic and photonic devices, and they possess temperature-dependent phases.[46] The properties of $CsPbX_3$ can be tuned by metal or mixing halides to enhance optoelectronic device applications such as LEDs, photo-detectors, and lasers.[52–76] Among $CsPbX_3$ (X = Cl, Br, I), $CsPbCl_3$ has a wider band gap and better thermal stability due to the value of binding energy of 64 meV,[47,48] which is preferable for the optomagnetic and optoelectronic,[49] single,[50] and multiphoton pumping-based laser devices.[51] The cubic bulk $CsPbBr_3$ has also temperature responses over the phase transition.[77–79] Halide exchange and mixing can ensure more suitable properties tuning of $CsPbBr_3$ for quantum dots due to high carrier transportability, reliable optoelectronic properties, and the enormous photoluminescence quantum yield, and greater constancy under humidity and thermal outbreaks.[80,81] $CsPbBr_3$ demonstrated a band gap of 2.30 eV,[82] and cubic bulk $CsPbI_3$ has a band gap of 1.73 eV.[83] It is a potential candidate for room temperature Si-based thin film perovskite heterojunction solar cells.[83,84] $CsPbI_3$ is a highly efficient thermally stable solar cell due to its relatively high light absorption coefficient, and carrier mobility in the visible region.[85] Organic–inorganic perovskites have a great tendency to dissolve under humidity at high temperature[86] and are greatly sensitive to light and heat[49] as well as the presence of toxic lead in these perovskites, which causes huge health issues to live creatures. It can be seen that $CsPbX_3$ (X = Cl, Br, I) are direct band gap semiconductors that absorb visible and ultraviolet light. Hence, these compounds are used in photovoltaic and optoelectronic devices. It should be remembered that pressure plays an important role in tuning the physical properties of any materials.[87–89] It treats phase transitions and is often reversible if the external conditions are the same in the complete cycle.[90,91] In this sense the high-pressure studies often offer fundamental insight into the optoelectronic properties of perovskite materials.[92–94] Perovskites are an advanced class of materials that have exhibited great potential in optoelectronic technologies thus all-inorganic perovskites have an extremely versatile crystal structure. Thus far, there are no such theoretical reports on the pressure-dependent comparative studies of the elastic, mechanical, electronic, optical, and photocatalytic properties of $CsPbX_3$.

In this work, for the first time, a pressure-dependent comparative study of the mechanical, elastic properties and electronic, optical, and photocatalytic properties has been performed through first-principles calculations based on the density functional theory (DFT). In this study, we tried to find out more stable and efficient materials among them to make a prediction for the proper selection of perovskite materials for electronic, photocatalytic, and optoelectronic applications.

2. Methodology

The bulk perovskites of $CsPbX_3$ (X = Cl, Br, I) exhibit cubic structure of space group *Pmm* (221), and the lattice constants

Table 1 Calculated optimized lattice parameters, volumes and band gap values of $CsPbCl_3$, $CsPbBr_3$ and $CsPbI_3$[a]

Materials	Method	Lattice parameters		Band gap, E_g (eV)	Bulk type
		a (Å)	V (Å^3)		
$CsPbCl_3$	Calc.	5.785	193	2.385	Cubic
	Theo.	5.62[a],5.743[b]		2.168[a], 2.202[b]	
		5.7[c], 5.7285[d]		2.4[c], 2.27[d], 2.72[i], 3.03[o]	
	Expt.	5.605[q]		2.98[m]	
				3.00[p]	
$CsPbBr_3$	Calc.	6.011	217	2.061	Cubic
	Theo.	6.013[b]		1.61[a], 2.30[f], 1.796[b], 2.30[e]	
		5.98[h]		1.74[g]	
		6.001[g]		1.86h, 2.30[o]	
	Expt.	5.87[a], 5.85[e]		2.28[i], 2.36[m]	
				2.33[p]	
$CsPbI_3$	Calc.	6.432	266, 260[j], 249[k]	1.784	Cubic
	Theo.	6.405[b], 6.38[j]		1.478[a], 1.479[b], 1.44[j]	
		6.24[a]		1.73[l]	
	Expt.	6.29[k]		1.77[m]	
				1.73[n]	

[a] Refs: a = [102], b = [103], c = [104], d = [105], e = [32], f = [82], g = [106], h = [107], i = [108], j = [109], k = [110], l = [83], m = [119], n = [120], o = [121], p = [122], q = [123].

are 5.734, 6.017, and 6.38, respectively (Table 1). To compare and analyze the data of the structural, mechanical, electronic, optical and photocatalytic properties, DFT calculations were performed using the CASTEP code in Materials Studio simulation software.[95–100] Valance shell and ion core electrostatic interactions of ingredient atoms were investigated under Generalized Gradient Approximation (GGA) of Perdew–Burke–Ernzerhof (PBE) with norm-conserving pseudo-potentials treatment but the mechanical properties were calculated using ultrasoft pseudopotentials for the better agreement with experimental data. The photocatalytic properties were also calculated from the electronic band structure calculations. Initially, we chose the cubic structure to carry out the numerical operations.

A primitive cell of $CsPbCl_3$ consisting 5 atoms was formed with 1 Cs atom that occupied the Wyckoff site (0, 0, 0), 3 Pb atoms at the site of (0.5, 0.5, 0.5) and 1 Cl atom at (0, 0.5, 0.5) fractional coordinates[101] as depicted in Fig. 1. The sets of valence shall are interacted as Cs: $5s^2\ 5p^6\ 6s^1$, Pb: $5s^2\ 5p^6\ 5d^{10}\ 6s^2\ 6p^2$, Cl: $3s^2\ 3p^5$, Br: $4s^2\ 4p^5$ and I: $5s^2\ 5p^5$. All the crystals were optimized using the same software functional treatments. $CsPbCl_3$ was simulated first by providing a lattice parameter as $a = 5.734$ (ref. 101) and the optimized structure with minimum formation enthalpy was confirmed with plane wave basic set *k*-points of $6 \times 6 \times 6$ and cut-off energy of 520 eV with SCF tolerance 2×10^{-6} eV per atom, convergence tolerance energy of 2×10^{-5} eV per atom as well as maximum force and stress 0.05 eV $Å^{-1}$and 0.10 GPa, respectively. The maximum atomic displacement was restricted up to 0.002 Å. We calculated the elastic, electronic, and optical properties for $CsPbBr_3$ and $CsPbI_3$ after replacing the Cl atom (100%) with Br and I atoms under the same conditions.

3. Results and discussion

3.1 Structural properties

The three phases (cubic, tetragonal and orthorhombic) of $CsPbCl_3$ were primarily chosen as the highest temperature phases of the cubic structure to carry out the numerical operations for high-temperature device applications. The optimized-cell structure of $CsPbCl_3$ was determined and then the Cl atom was replaced by Br and I atoms, which were then optimized for $CsPbBr_3$ and $CsPbI_3$ perovskite structures. Fig. 1(a)–(c) represent the optimized crystal structures of $CsPbCl_3$, $CsPbBr_3$ and $CsPbI_3$. The optimized cell parameters for the corresponding perovskites are represented in Table 1. From Table 1, it can be seen that after several *k*-points tests the optimized lattice parameter $a = b = c$ of $CsPbCl_3$ was 5.785 Å, which was elongated about 3.9% and 11.2% after the replacement of halide Cl atom by Br and I atoms and the obtained values were in a great agreement with other theoretical and experimental values.[32,82,83,102–110,123] From the cell parameters and volumes of

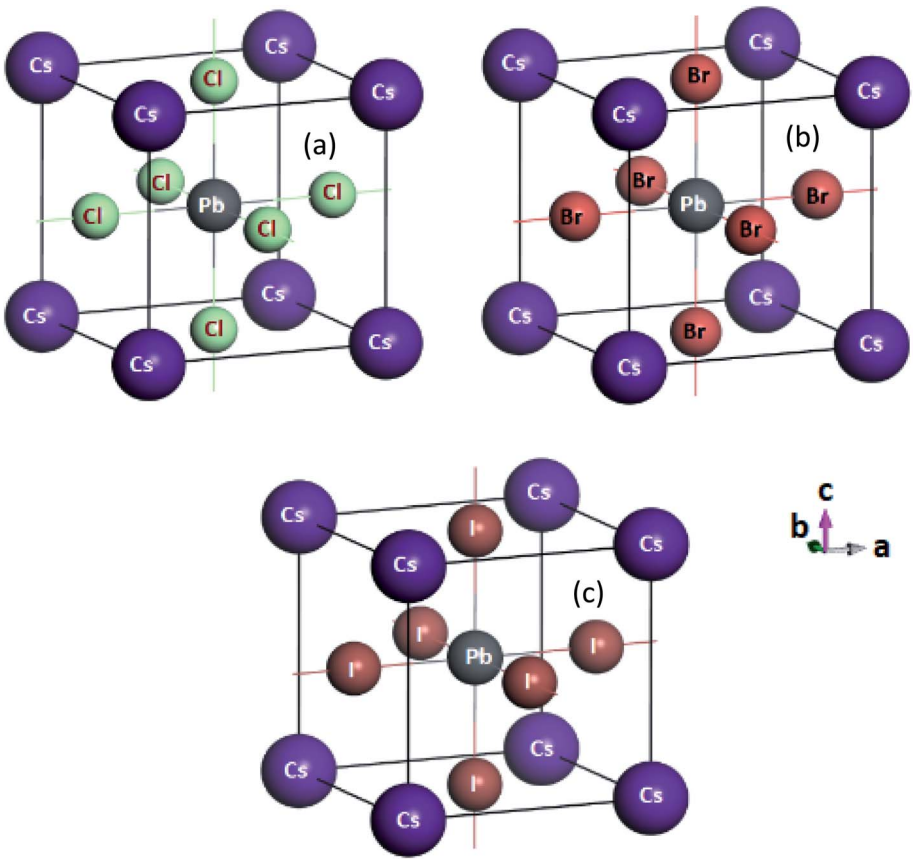

Fig. 1 Cubic structure of (a) $CsPbCl_3$ (b) $CsPbBr_3$ and (c) $CsPbI_3$ are depicted with atomic orientations.

Table 2 Calculated pressure independent (at 0 GPa) elastic constants C_{ij} (GPa), elastic moduli B, G, E (GPa), Pugh's ratio B/G, Poisson's ratio σ, and machinability index $\mu_M = B/C_{44}$ and elastic anisotropy factor A, melting temperature T_m for $CsPbCl_3$, $CsPbBr_3$ and $CsPbI_3$[a]

Materials	C_{11}	C_{12}	C_{44}	B	G	E	B/G	σ	μ_M	A	T_m
$CsPbCl_3$	48.353, 52.941[n]	7.881, 11.700[n]	4.921, 4.800[n]	21.372, 25.447[n]	9.052, 9.027[n]	23.799	2.361, 1.234[n]	0.314	4.342	0.243	838.7
$CsPbBr_3$	51.946	16.479	4.189	28.302	7.819	21.479	3.619	0.374	6.756	0.236	860.0
$CsPbI_3$	39.323	6.754	5.352	17.61	8.522	22.015	1.811	0.292	3.289	0.328	785.4

[a] Ref: n = [115].

$CsPbX_3$ (X= Cl, Br, I) results, a relation can be expressed as $CsPbCl_3$ < $CsPbBr_3$ < $CsPbI_3$ (Table 1) with volume increments of 12.4% and 37.8% for $CsPbBr_3$ and $CsPbI_3$, respectively.

3.2 Mechanical properties

The mechanical properties of the cubic crystals of $CsPbX_3$ were explicitly and implicitly calculated using three independent elastic tensors C_{11}, C_{12} and C_{44}. The calculated values are represented in Table 2 and shown graphically in Fig. 2(a) for the isostructural of $CsPbCl_3$, $CsPbBr_3$, and $CsPbI_3$. Mechanical stability was justified under Born criteria for these crystals[111] and it is clearly seen that all are mechanically stable because they satisfy the condition $C_{11} + 2C_{12} > 0$, $C_{44} > 0$ and $C_{11} - C_{44} > 0$ as well as another stability condition of $C_{12} < B < C_{11}$.[106] All of these in the bulk form are elastically anisotropic, confirmed by the relation $2C_{44} = C_{11} - C_{12}$ (ref. 112) and reconfirmed by non-zero Zener's anisotropy factor A.[113,114] The $C_{11} > C_{12} > C_{44}$ conditions show that the materials resist longitudinal deformation of more than shape deformation, where the largest value of C_{11} for $CsPbBr_3$ offers more resistance to longitudinal deformation. Young's modulus (E) is an indication of the degree of resistance offered by a material to longitudinal tension.[106] A comparative data set of E's (Table 2) could be an inspiration for

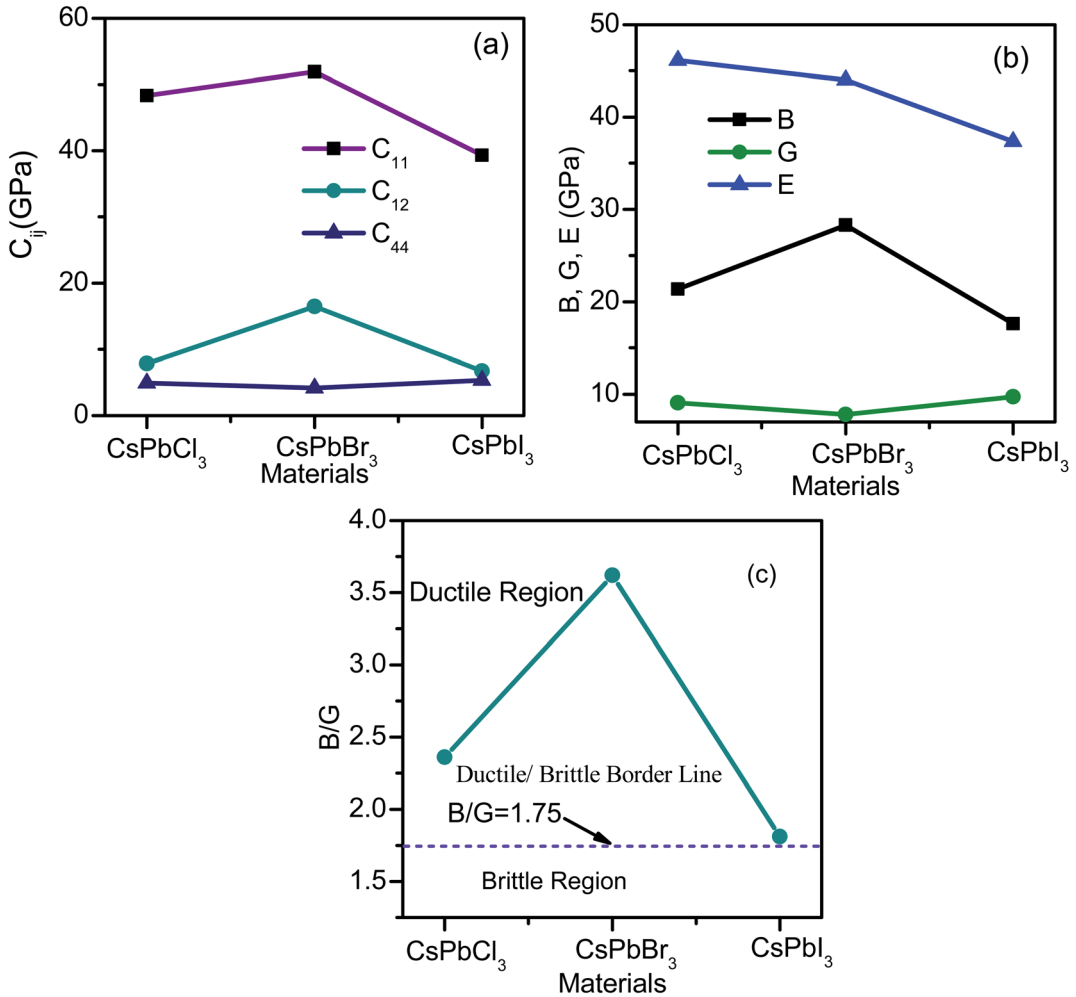

Fig. 2 Elastic tensors C_{ij}, modulus of elasticity B, G, and E are plotted in (a) and (b) respectively. Pugh's ratio is shown in (c) for $CsPbX_3$.

conducting further research on $CsPbBr_3$ for band gap tailoring and other purposes due to the comparatively high value of E. Pressure responses of $CsPbX_3$ are depicted in Fig. 2(b) with B, G, E data. A comparative study of Cauchy pressure $C_{12} - C_{44}$ (ref. 115) of the tabulated data shown in Table 1 confirms the brittle-like nature of $CsPbCl_3$ > $CsPbBr_3$ > $CsPbI_3$, which can be reconfirmed from the values of Pugh's ratio $B/G < 1.75$ for all structures,[116] which is shown in Fig. 2(c). It offers a completely new result from other researchers' findings,[117,118] which may open a new opportunity to observe the material insight. $CsPbBr_3$ offers a larger value of bulk modulus, whereas $CsPbCl_3$ offers the least value, thus the compressibility of these perovskites can be ordered as $CsPbBr_3$ < $CsPbI_3$ < $CsPbCl_3$.

The elastic and universal anisotropy factors A and A^U were calculated using the following relations[115,116] as

$$A = \frac{2C_{44}}{C_{11} - C_{12}} \text{ and } A^U = 5\frac{G_V}{G_R} + \frac{B_V}{B_R} - 6 \geq 0$$

The values of Zener's anisotropy factor, A, for all structures were less than unity. Any deviation from unity confirms the elastic anisotropic property.[117] For these materials, the order of anisotropy can be obtained as $CsPbBr_3$ > $CsPbI_3$ > $CsPbCl_3$ (Table 2). The melting point temperatures (T_m) were calculated using the following empirical formula proposed by Fine *et al.*[118]

$$T_m = 553 + 5.91C_{11}$$

From Table 2, it is obvious that $CsPbBr_3$ possesses the highest melting temperature due to the highest C_{11} and the comparison suggests that $CsPbBr_3$ is a better choice for high-temperature efficiency and potential applications in comparison to the other two. The value of the machinability index indicates the suitability of the materials for industrial applications, whereas $CsPbBr_3$ shows dominating nature over $CsPbCl_3$ and $CsPbI_3$ (Table 2) though its H_v value is the lowest one.

The calculated elastic constants are tabulated in Table 3. The values of the calculated elastic constants are positive and satisfy the Born stability criteria, which implies that the compounds are mechanically stable. The calculated elastic constants for $CsPbCl_3$ are in good agreement with the available theoretical results reported in the literature.[115] It should be noted that the mechanical instability is responsible for the negative values of C_{44} and B/C_{44}, whereas stability can be satisfied by the value of $C_{44} > 0$. From Table 3 and Fig. 3(a), we observed that $CsPbCl_3$ and $CsPbBr_3$ lose mechanical stability at an applied pressure above 20 GPa and 25 Gpa, respectively, while $CsPbI_3$ can tolerate more pressure and shows stability up to the hydrostatic pressure of about 75 GPa. The mechanical instability was confirmed

Table 3 Calculated pressure-dependent elastic constants C_{ij} (GPa), elastic moduli B, G, E (GPa), Poisson's ratio σ, and machinability index $\mu_M = B/C_{44}$ and Pugh's ratio B/G for $CsPbCl_3$, $CsPbBr_3$ and $CsPbI_3$

Materials	P	a (Å)	V (Å^3)	C_{11}	C_{12}	C_{44}	B	G	E	σ	B/C_{44}	B/G
$CsPbCl_3$	0	5.734	188.526	48.353	7.881	4.921	21.372	9.052	23.796	0.314	4.343	2.361
	5	5.446	161.53	97.069	16.589	4.065	43.416	12.44	34.068	0.369	10.68	3.489
	10	5.271	146.485	145.49	29.864	2.916	68.406	14.79	41.382	0.399	23.458	4.625
	15	5.151	136.698	175.01	27.907	1.684	76.941	16.6	46.453	0.399	45.689	4.635
	20	5.052	128.959	214.4	36.143	0.483	95.561	18.37	51.796	0.409	197.85	5.201
	25	4.972	122.947	249.95	43.191	−0.716	112.11	19.86	56.26	0.416	−156.58	5.644
	30	4.903	117.891	281.84	47.262	−2.008	125.46	21.16	60.103	0.42	−62.477	5.928
$CsPbBr_3$	0	6.014	217.613	51.946	16.479	4.189	28.301	7.819	21.478	0.373	6.756	3.619
	5	5.663	181.623	90.465	13.995	3.612	39.485	11.56	31.601	0.366	10.931	3.415
	10	5.473	163.947	125.74	14.119	2.887	51.327	14.35	39.39	0.372	17.778	3.575
	15	5.339	152.189	173.83	28.697	2.141	77.074	16.91	47.262	0.397	35.999	4.558
	20	5.235	143.502	211.2	35.276	1.285	93.918	19.04	53.501	0.405	73.087	4.932
	25	5.151	136.732	248.17	43.089	0.334	111.45	20.89	58.971	0.411	333.68	5.336
	30	5.079	131.056	283.31	49.763	−0.661	127.61	22.6	64.025	0.416	−193.06	5.646
$CsPbI_3$	0	6.403	262.567	39.323	6.754	5.352	17.61	8.521	22.012	0.291	3.29	2.066
	5	5.985	214.423	81.669	12.258	4.671	35.395	11.91	32.136	0.348	7.577	2.97
	10	5.761	191.205	119.43	15.974	1.343	50.461	11.85	32.966	0.391	37.573	4.258
	15	5.608	176.452	170.4	27.372	6.436	75.048	21.29	58.362	0.37	11.66	3.524
	20	5.498	166.228	207.43	35.467	5.792	92.787	23.55	65.146	0.382	16.019	3.939
	25	5.405	157.935	238.25	38.761	3.174	105.26	23.49	65.593	0.396	33.162	4.48
	30	5.323	150.823	288.88	50.853	7.061	130.2	31.58	87.658	0.387	18.438	4.122
	35	5.258	145.437	323.53	58.817	6.712	147.06	33.9	94.429	0.392	21.909	4.338
	40	5.202	140.813	357.61	66.848	6.365	163.77	36.14	100.99	0.397	25.729	4.531
	45	5.152	136.783	388.58	72.781	5.468	178.05	37.67	105.58	0.401	32.561	4.725
	50	5.105	133.092	419.99	79.415	3.509	192.94	38	106.96	0.407	54.984	5.078
	55	5.063	129.827	449.5	84.787	1.322	206.36	37.96	107.31	0.413	156.1	5.435
	60	5.024	126.86	483.76	93.126	0.972	223.34	40.16	113.67	0.415	229.77	5.56
	65	4.988	124.135	523.28	103.91	3.342	243.7	45.7	129.02	0.411	72.92	5.333
	70	4.956	121.731	560.19	114.31	4.659	262.93	49.82	140.57	0.41	56.435	5.278
	75	4.925	119.505	588.96	119.87	2.623	276.23	49.87	141.1	0.414	105.31	5.539
	80	4.896	117.42	615	124.42	−0.964	287.95	47.96	136.32	0.421	−298.7	6.003

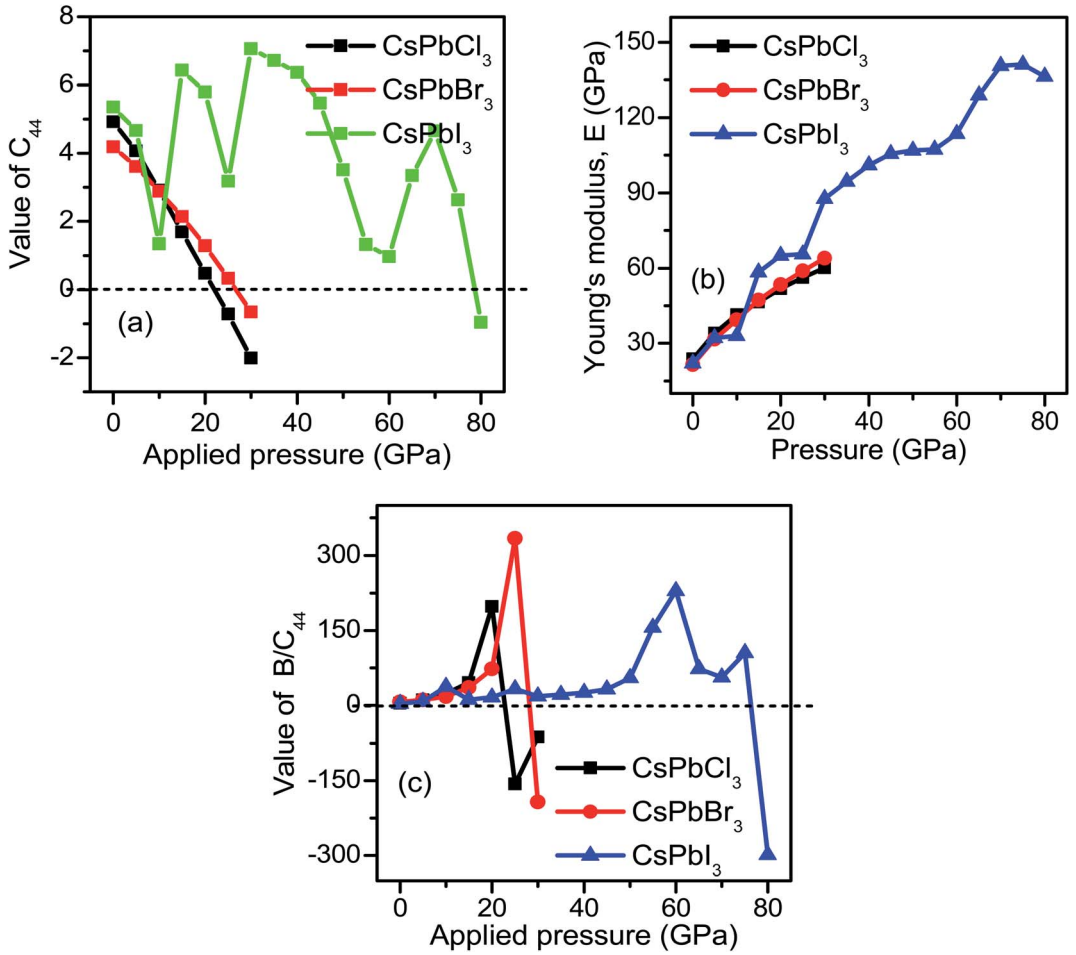

Fig. 3 Pressure-dependent (a) elastic tensor C_{44}, (b) Young's modulus (E), and (c) machinability index ($\mu_M = B/C_{44}$) are plotted for $CsPbX_3$.

from the negative value of C_{44} corresponding to the threshold pressures for individual perovskites. From the above discussion and the obtained results, the stability order of the three compounds under applied pressure can be followed as $CsPbI_3$ > $CsPbBr_3$ > $CsPbCl_3$, but $CsPbI_3$ remains stable under hydrostatic pressure approximately three times more than that of $CsPbCl_3$ (Table 3 and Fig. 3(c)). The Poisson's ratio of the system was calculated using the following formula.

$$\sigma = \frac{3B - 2G}{2(3B + G)}$$

The calculated values are also included in Table 3. It is obvious that with the increase in hydrostatic pressure, the value of the Poisson's ratio σ increases for $CsPbX_3$. It is well known that σ can separate crystalline solids as brittle and ductile at the borderline value of 0.26. From Table 3, it can be clearly evident that all the structures possessed values greater than 0.26, indicating that they must be quite ductile in nature. Among them, $CsPbI_3$ is more ductile as it has more pressure tolerance. Bulk to shear modulus ratio (B/G) with the critical value of ductility of 1.75 served as the borderline between the ductile and brittle behaviors of crystalline solids. It also predicted a more ductile behavior of $CsPbI_3$.

$$E = \frac{9GB}{3B + G}$$

Young's modulus, E measures the stiffness against longitudinal deformation as well as thermal shock resistance of the materials. A larger value of E indicates a smaller thermal resistance. The thermal shock resistance order under different pressure conditions followed the order $CsPbCl_3$ > $CsPbBr_3$ > $CsPbI_3$ (Fig. 3(b)).

3.3 Electronic properties

The energy band diagram with k-points in Brillouin zone sampling represents the energy band gap of a material. Fig. 4(a)–(c) represents the electronic band structures of $CsPbX_3$. The energy differences between the top of the valence band (VB) and the bottom of the conduction band (CB) along the same point of momentum space (at the R point) for all structures provides evidence for the existence of a direct band gap. Electronic transition in the direct band gap material offers less momentum loss for carrier propagation as the phonon contributions are negligible for pair creation. From Fig. 4, it is clearly seen that the valence shells are extended from −5 eV up to 0 eV, where 0 eV energy levels (green lines) represent the

Fermi levels (E_F). The electronic shells above the E_F form conduction bands, which have been extended from 0 eV up to 5 eV. From Fig. 4(a)–(c), it is seen that $CsPbCl_3$, $CsPbBr_3$ and $CsPbI_3$ have direct band gaps with values of 2.385 eV, 2.061 eV and 1.784 eV, respectively, where $CsPbCl_3$, $CsPbBr_3$ and $CsPbI_3$ show the carrier transitions for green, orange and red emissions

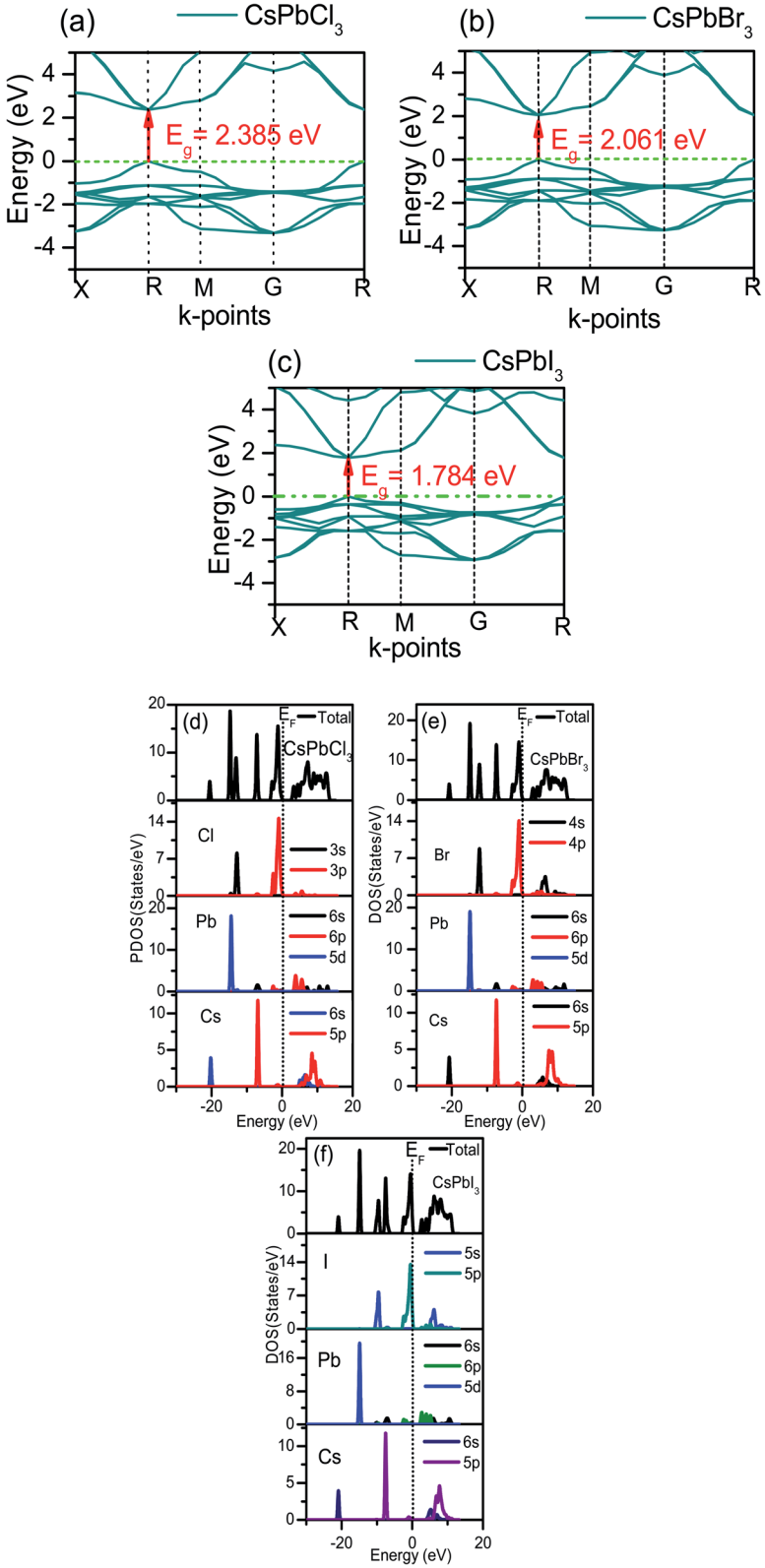

Fig. 4 Energy band diagram with k-points for (a) $CsPbCl_3$, (b) $CsPbBr_3$ and (c) $CsPbI_3$, and density of states (DOS) with corresponding energy of the ingredient atoms of (d) $CsPbCl_3$, (e) $CsPbBr_3$ and (f) $CsPbI_3$ calculated in GGA-PBE treatments.

of visible spectra, respectively. Solar irradiance on earth's surface is of maximum photon flux density for green wavelength and appreciably high enough for orange as well as red spectra of the visible region.[105]

The obtained values of the band gap are listed in Table 1. By comparing the band gaps shown in Table 1, it is evident that the value of $CsPbCl_3$ is closest to the theoretical reported values of 2.168 eV,[102] 2.202 eV,[103] 2.40 eV,[104] and 2.27 eV (ref. 102) but it is (2.385 eV) smaller than the theoretical value of 3.03 eV (ref. 121) and experimental value of 3.0 eV.[119,122]

From Table 1 it is clearly seen that the calculated band gap of $CsPbBr_3$ is 2.061 eV, whereas the band gaps of $CsPbBr_3$ are reported as 1.796 eV,[103] 1.74 eV,[106] 2.30 eV,[32,82,121] 2.36 eV,[119] 2.33eV,[122] 1.86 eV (ref. 107) and 2.28 eV.[108] Thus, our findings are in good agreement and very close to the other theoretical and experimental findings.[32,82,103,106–108,121,122] Importantly, we were able to tune the band gap of $CsPbBr_3$ to 2.061 eV, which is excellent suitable for optoelectronic and PV cell applications, whereas, our calculated E_g value for $CsPbI_3$ was obtained to be 1.784 eV, which is in excellent agreement with the experimental value of 1.77 eV (ref. 119) and theoretical value of 1.73 eV (ref. 83 and 120) as well as more reliable than others theoretical observation of ~1.478 eV,[102] 1.479 eV,[103] 1.44 eV (ref. 109) but very close to the experimental value (Table 1).[83,102,103,109] It should be noted that the theoretical band gap obtained using PBE–GGA is a little bit underestimated compared to the experimental value, which could be due to the error in GGA.[119–123] It can be seen that when Cl is partially replaced by Br and I atoms, the band gap decreases because of an increase in the atomic size. In all cases, the origin of some discrepancies with experimental values may arise from the drawbacks of the calculative process of the first principal calculations. From Fig. 4(a)–(c), it is explicitly clear that the top of the VB is well dispersive than the bottom of the CB, which indicates that the photo-generated holes possess lower effective mass. A lower carrier effective mass corresponds to higher carrier mobility. As such, the photo-generated holes in the VB can transfer more rapidly to the surface of $CsPbX_3$ to participate in conduction and in photo-catalytic reactions. This nature of the charge carriers for $CsPbX_3$ systems supports the p-type conduction of $CsPbCl_3$, $CsPbBr_3$, and $CsPbI_3$. The curvature of the valence band maxima shows a decrement with the replacement of Cl by Br and I. The hole mobility decreases with the insertion of Br and I in the place of Cl in $CsPbCl_3$.

Atomic contributions to the band structure formation are shown in terms of density of states (DOS) for individual atoms and the total densities of states (TDOS) for all atoms are shown in Fig. 3(d–f) for $CsPbX_3$ perovskites. From Fig. 4(d), it is evident that the DOS of $CsPbCl_3$ can be divided into six major regions. The first region (Fig. 3(d)) −21.14 eV to −19.54 eV is mainly arising due to the Cs-6s orbital state, the second region −15.08 eV to −13.54 eV is due to the Pb-5d state, the third region −13.38 eV to −12.23 eV is due to Cl-3s, the fourth region −7.33 eV to −5.82 eV is due to the hybridization of Cs-5p and Pb-5d states and the fifth region lies between −3.16 eV to 0 eV below the E_F level, which is called the top of the valence band and is originated from the 3p orbital of Cl atom. Whereas the

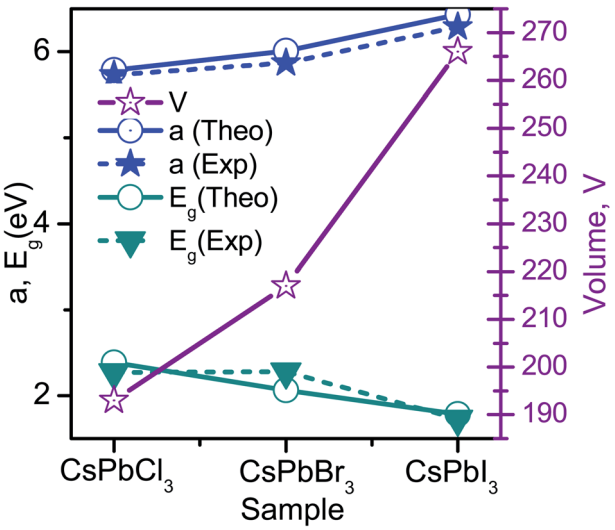

Fig. 5 Comparative presentation of theoretical and experimental values of lattice parameters and band gap values for $CsPbX_3$ (X = Cl, Br, I).

conduction band that lies between 2.38 eV and13.24 eV, above the E_F level, originated from the hybridization of the 6p orbital of Cs and 6p orbital of Pb and 3p orbital of Cl atoms. In a similar way, for $CsPbBr_3$ the core VB originated from the mixing of Cs-3p, Pb-5d, Br-3s, Cs-5p, and Pb-5d and the top of the valence band originated from the 4p state of Br atom and the CB band arise from the hybridization of the 6p orbital of Cs and the 6p orbital of Pb and the 4p orbital of Br atoms (Fig. 4(e)). For the $CsPbI_3$ system, the core VB originated from Cs-3p, Pb-5d, I-3s, Cs-5p, and Pb-5d and the top of the valence band originated from the 5p state of the I atom and CB occurred from the predominant hybridization of Cs-6p, Pb-6p and I-5p orbitals of Cs, Pb, I atoms (Fig. 4(f)). From the atomic contribution plots, it is clear that Pb and halogen atoms have a major contribution to the valence and conduction bands, which reduces the band gap energy. The s and p states of Pb and the p state of the halogens play a major role in the reduction of band gap energy as shown in Fig. 4(d)–(f). The order of decrement can be assigned as $CsPbCl_3$ > $CsPbBr_3$ > $CsPbI_3$ (Fig. 5).

3.4 Optical properties

Many application fields, such as absorbers, reflectors, optical coatings, and different optoelectronic devices of materials are examined from their optical responses. In the presence of an external electromagnetic wave, the photonic interactions of the material can provide information on the properties and application predictions as a function of energy. These properties are analyzed for electronic transitions between occupied and empty states, band structures, bond types as well as internal structures of the materials according to their optical spectra. The frequency-dependent complex dielectric function is followed by the Kramers–Kronig transformation as $\varepsilon(\omega) = \varepsilon_1(\omega) + i\varepsilon_2(\omega)$, which is also related to the representation of relative permittivity. The imaginary part of this complex function is,

$$\varepsilon_2(\omega) = \frac{2e^2\pi}{\Omega\varepsilon_0}\sum_{k,v,c} k\psi_k^c\left|\hat{u}\cdot\hat{r}\left|\psi_k^v\right|\right|^2\delta\left(E_k^c\right) - E_k^v - (E)$$

where $\omega = 2\pi\nu$ is the frequency of the incident photon and e, $\hat{u}$, $\hat{r}$ are the electronic charge, polarization vector of the incident field, and radius vector, respectively. Whereas, $\Psi_k{}^c$ and $\Psi_k{}^v$ are the wave functions of the conduction and valence bands at K, respectively. Using ε_1 and ε_2, other optical properties such as absorption coefficient $\alpha(\omega)$, optical conductivity $\sigma(\omega)$, loss function $L(\omega)$, reflectivity $R(\omega)$ and refractive index $n(\omega)$ can be calculated[118] using the following expressions.

$$\sigma(\omega) = \frac{\omega\varepsilon_2}{4\pi} = \hbar\omega$$

$$L(\omega) = \frac{\varepsilon(\omega)}{\varepsilon_1(\omega)^2 + \varepsilon_2(\omega)^2}$$

$$R(\omega) = \left|\frac{\sqrt{\varepsilon}(\omega) - 1}{\sqrt{\varepsilon}(\omega) + 1}\right|^2$$

$$n(\omega) = \left|\frac{\varepsilon_1(\omega)}{2} + \frac{\sqrt{\varepsilon_1(\omega)^2 + \varepsilon_2(\omega)^2}}{2}\right|^{\frac{1}{2}}$$

The dielectric function is a fundamental parameter that is related to the charge-carrier regeneration rate of certain materials used in the solar cell.[124,125] It gives a clear idea of the performance of optoelectronic devices.[126] Higher dielectric constant values of the perovskite solar cells can lead to lower recombination rates. Fig. 6(a) shows the imaginary parts of the dielectric function of $CsPbX_3$ perovskites. The real part of the dielectric function shows a higher value at low photon energy and then decreases rapidly with the increase of photon energy. It is well known that a perovskite material with such a higher value of the real part of the dielectric function exhibits a lower band gap,[127] which is also seen in the electronic band structure. On the other hand, the values of the imaginary part of the dielectric function decrease to zero at a higher photon energy region. It should be noted that there are few peaks arising at 3.9,

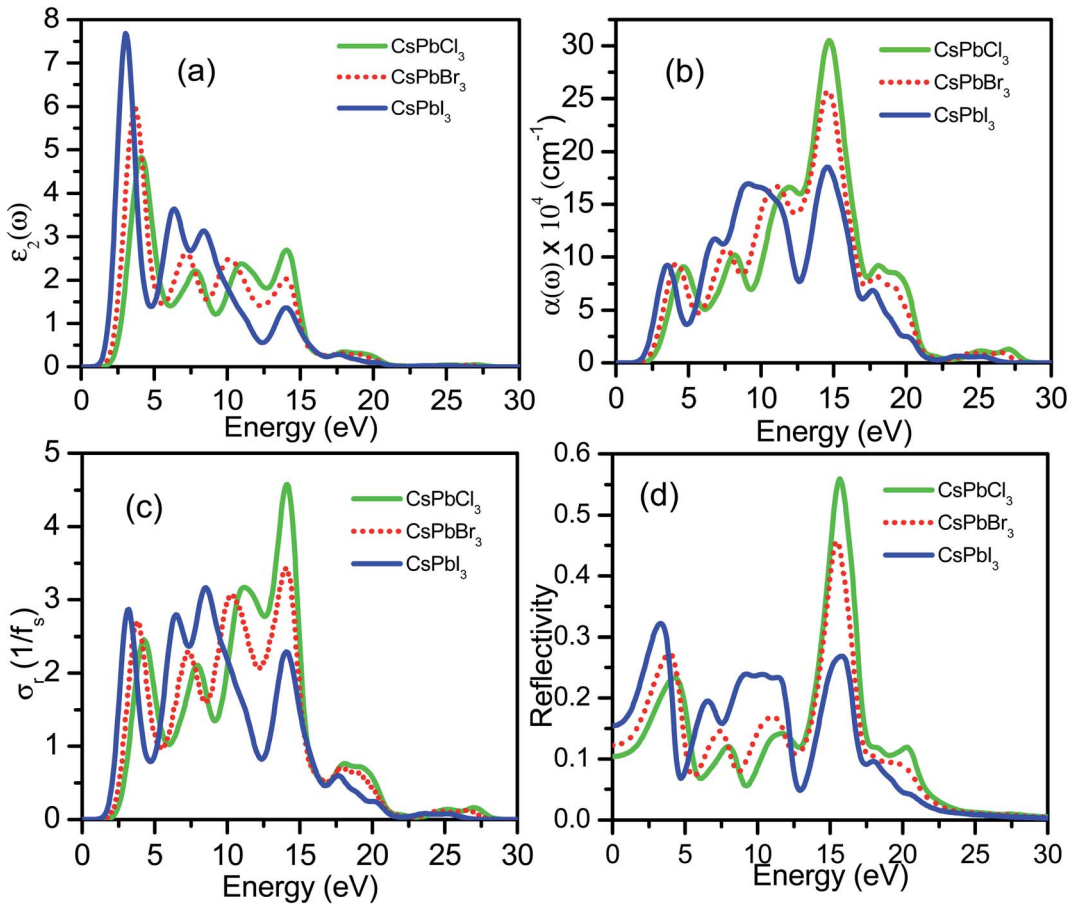

Fig. 6 Optical responses in terms of dielectric functions (a), (b) absorption coefficients, (c) conductivity and (d) reflectivity of $CsPbCl_3$, $CsPbBr_3$ and $CsPbI_3$ are shown with green, dotted red and blue lines, respectively.

7.8, 11.0 and 14.1 eV for $CsPbCl_3$; 3.5, 7.3, 10.3 and 13.9 eV for $CsPbBr_3$; and 3.0, 6.3, 8.5 and 13.9 eV for $CsPbI_3$. The first peak is due to the generation of the electron–hole pairs for conduction. The 2nd and 3rd peaks are due to the interband optical transitions from the valence bands to the conduction bands. The fourth peak around 14.0 eV is due to the collecting excitons from the free carriers, which is the so-called plasma frequency and the peak is called the plasmon peak. These irregular photo responses of the materials cause the difference in band gaps among them.

It is well known that the performance of solar cells is determined by various optical properties, among them the absorption coefficient (α) is the crucial property. The variation of optical absorption of $CsPbX_3$ perovskites can be seen in Fig. 6(b). The value of α of the I-based perovskite demonstrates its maximum intensity in the ultraviolet region compared to that of Br and Cl-based perovskites. The first peak of α offers an optical transition of electrons from Cl-3p of the valence band to Pb-6p of the conduction band at higher energy compared to that of the interband transitions of electrons in the case of $CsPbBr_3$ and $CsPbI_3$. The optical band gaps can be seen from the absorption peaks of corresponding materials as E_g ($CsPbCl_3$)> E_g ($CsPbBr_3$) > E_g ($CsPbI_3$), which is coherent with the calculated values of E_g of $CsPbX_3$ perovskites (Table 1). The highest absorption peaks for all materials occurred at the same energy of 14.6 eV (Fig. 6(b)).

Fig. 6(c) shows the real part of photoconductivity. From the figure, it is evident that if the absorption of photons enhances, the rate of photoconductivity tends to increase. Thereby, greater absorption and more photoconductivity are observed in the I-based perovskite compound relative to the Br and Cl-based perovskite compounds. The photoconductivity comparison of these materials shows some peaks over a wide range of energy spectra. The conductivity initiatives and the first peaks are ordered in terms of the energy as σ ($CsPbI_3$) > σ ($CsPbBr_3$) > σ ($CsPbCl_3$). Photoconductivity increases at the energy edges 4.2, 7.8, 11.3 and 14.1 eV for $CsPbCl_3$, 3.8, 7.3, 10.2 and 14.1 eV for $CsPbBr_3$ and 3.0, 6.4, 8.3 and 14.1 eV for $CsPbI_3$ as a result of photonic energy absorption, which is shown in Fig. 6(c).

Reflectivity is an important optical property that determines the surface nature of the materials for optoelectronic and solar cell applications.[128] Fig. 6(d) shows the reflectivity spectra of $CsPbX_3$ perovskites. From these data, it can be seen that the reflectivity is very low for all the studied cubic perovskite compounds; however, the reflectivity shows maximum for $CsPbI_3$ and minimum for $CsPbCl_3$ perovskites, at the optical range. Some peaks arise in each spectrum, which are the responses still true for infra-red and visible regions. In the visible region, the first peaks are observed at 4.2, 3.8 and 3.3 eV for $CsPbCl_3$, $CsPbBr_3$ and $CsPbI_3$, respectively. Some other peaks are observed at 7.8, 11.5, 15.6, 20.4 eV for $CsPbCl_3$, at 7.3, 10.9, 15.4 eV for $CsPbBr_3$ and at 6.3, 9.0, 11.3, 15.8 eV for $CsPbI_3$. From the comparison of reflectivity, it is clearly seen that $CsPbI_3$ shows the most homogeneous response over a wide energy range in the ultraviolet region.

3.5 Redox potentials: photocatalytic activity

The photocatalytic activity of material depends highly on the suitable band gap, the recombination rate of carriers, and proper redox potentials. An idealization arises from a narrow band gap, low recombination rate with long-life carriers, and proper redox potentials of the compounds irradiated under visible light. The redox ability for visible light exposure can be calculated theoretically by aligning the CBM and VBM compared to the water reduction/oxidation potential level (Fig. 7). The positions of CBM and VBM can theoretically be predicted by employing the following equations,[129]

$$E_{CB} = X - E_e + 0.5E_g \text{ and } E_{VB} = E_{CB} + E_g$$

where E_{CB} and E_{VB} are the CB and VB edge potentials, X is the absolute electronegativity of $CsPbX_3$. Absolute or Mulliken electronegativity is numerically equal to the geometric mean of electronegativities of ingredient elements where the first ionization energy and the atomic electron affinity are well employed.[130] E_g is the electronic band gap value and E_e is the energy of free electrons on the hydrogen scale (4.5 eV).

The calculated electronegativities, X are 5.56 eV, 5.17 eV, and 4.83 eV, whereas the electronic band gaps E_g are observed (in Fig. 4) as 2.385 eV, 2.061 eV and 1.784 eV for $CsPbCl_3$, $CsPbBr_3$ and $CsPbI_3$ respectively. The CBM potentials occurred at −0.24 eV, −0.36 eV, −0.57 eV *versus* NHE and the VBM potentials were at 2.15 eV, 1.70 eV and 1.22 eV for $CsPbCl_3$, $CsPbBr_3$ and $CsPbI_3$, respectively. By comparing these values, it is seen that the CBM-negative responses can be ordered as $CsPbCl_3$ < $CsPbBr_3$ < $CsPbI_3$ to the H^+/H_2 level and the VBM can be ordered as $CsPbCl_3$ > $CsPbBr_3$ > $CsPbI_3$ with positive to O_2/H_2O (1.23 eV). Analysis of these results provides explicit evidence that $CsPbCl_3$ is one of the best candidates for its strong ability of water oxidation from the thermodynamics aspect generating O_2, whereas $CsPbI_3$ is the best candidate as an H_2 producing agent

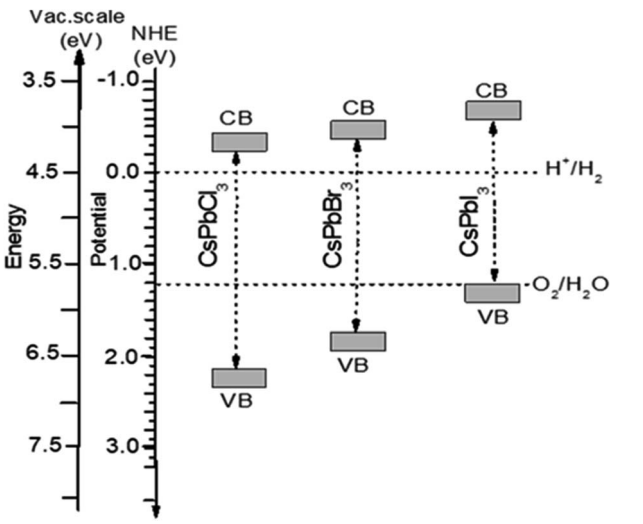

Fig. 7 Band edge potentials of $CsPbX_3$ (X = Cl, Br, I) for CBM and VBM estimated under GGA–PBE functions by applying the band structure and band gap values.

due to its strong redox potential. In contrast, $CsPbBr_3$ was found to be the best performer for the photocatalytic process in the visible region due to nearly equal effectiveness to both the oxidation and reduction processes.

4. Conclusions

The above mentioned properties investigation compares the applicability of these materials in optoelectronic, photocatalytic, and photovoltaic (PV) devices. We calculated structural, and elastic properties to determine the better agreement of damage-tolerance and electronic and optical responses for suitable device applications. The optimized lattice constant and elastic constant showed excellent agreement with the experimental data whereas some properties were found to be much better when compared to other theoretical reports. $CsPbBr_3$ is thermally more stable but more brittle than the other two perovskites. From a comparative study, it is seen that $CsPbCl_3$, $CsPbBr_3$, and $CsPbI_3$ are suitable for green, orange, and red emissions, respectively, of the optical spectra, owing to the proper electronic band gap. Theoretically, it was observed that $CsPbI_3$ is the best photocatalyst for the hydrogen evolution reaction and $CsPbBr_3$ is the most stable photocatalyst due to its nearly balanced oxidation and reduction potentials, but $CaPbCl_3$ is better for O_2 production. Thus, pressure can be employed to tune the properties of materials by adjusting their lattice parameters, electronic orbitals, crystal structure interatomic distances, and bonding patterns for efficient electronic and optoelectronic applications.

Author contributions

M. Aktary performed conceptualization, designed the study, interpreted the data, and wrote the manuscript. M. Kamruzzaman helped study, data analysis, and wrote the manuscript. R. Afrose Helped us to understand software, DFT calculations, data curation, writing-review, writing and editing the manuscript.

Conflicts of interest

The authors declare no competing financial interests.

Acknowledgements

The authors would like to thank the Department of Physics, Begum Rokeya University, Rangpur, Rangpur-5400 for supporting the computer facility. M. Aktary would like to dedicate this paper to her beloved father Hasinur Rahman for his kind and cordial supports during this research.

References

1 A. Hagfeldt, G. Boschloo, L. Sun, L. Kloo and H. Pettersson, *Chem. Rev.*, 2010, **110**, 6595–6663.
2 J. Burschka, N. Pellet, S.-J. Moon, R. Humphry-Baker, P. Gao, M. K. Nazeeruddin and M. Grätzel, *Nature*, 2013, **499**, 316.
3 M. Liu, M. B. Johnston and H. J. Snaith, *Nature*, 2013, **501**, 395.
4 W. B. Xiao, M. M. Liu and C. Yan, *J. Nanoelectron. Optoelectron.*, 2017, **12**, 189–195.
5 H.-J. Park, K.-H. Lee, B. Kumar, K.-S. Shin, S.-W. Jeong and S.-W. Kim, *J. Nanoelectron. Optoelectron.*, 2010, **5**, 135–138.
6 A. Yella, H. W. Lee, H. N. Tsao, C. Y. Yi and A. K. Chandiran, *Science*, 2011, **334**, 629.
7 N. J. Jeon, J. H. Noh, W. S. Yang, Y. C. Kim, S. Ryu, J. Seo and S. I. Seok, *Nature*, 2015, **517**, 476.
8 M. M. Lee, J. Teuscher, T. Miyasaka, T. N. Murakami and H. J. Snaith, *Science*, 2012, **338**, 643–647.
9 C. H. Chiang, M. K. Nazeeruddin, M. Gratzel and C. G. Wu, *Energy Environ. Sci.*, 2017, **10**, 808–817.
10 T. R. Cook, D. K. Dogutan, S. Y. Reece, Y. Surendranath, T. S. Teets and D. G. Nocera, *Chem. Rev.*, 2010, **110**, 6474–6502.
11 J. H. Bang and P. V. Kamat, *ACS Nano*, 2009, **3**, 1467–1476.
12 Z. Pan, K. Zhao, J. Wang, H. Zhang, Y. Feng and X. Zhong, *ACS Nano*, 2013, **7**, 5215.
13 M. Jorgensen, K. Norrman and F. C. Krebs, *Sol. Energy Mater. Sol. Cells*, 2008, **92**, 686–714.
14 K. Yoshikawa, H. Kawasaki, W. Yoshida, T. Irie, K. Konishi, K. Nakano, T. Uto, D. Adachi, M. Kanematsu, H. Uzu and K. Yamamoto, *Nat. Energy*, 2017, **2**, 17032.
15 M. D. Kelzenberg, S. W. Boettcher, J. A. Petykiewicz, D. B. Turner-Evans, M. C. Putnam, E. L. Warren, J. M. Spurgeon, R. M. Briggs, N. S. Lewis and H. A. Atwater, *Nat. Mater.*, 2010, **9**, 239–244.
16 A. Kojima, K. Teshima, T. Miyasaka and Y. Shirai, *210th ECS Meeting*, ECS, 2006.
17 A. M. M. Tanveer Karim, M. K. R. Khan, M. S. Hossain, M. Kamruzzaman, M. Azizar Rahman and M. Mozibur Rahman, *Mater. Sci. Eng., B*, 2020, **259**, 114599.
18 A. Kojima, K. Teshima, Y. Shirai and T. Miyasaka, *J. Am. Chem. Soc.*, 2009, **131**, 6050–6051.
19 M. Jošt, E. Köhnen, A. B. Morales-Vilches, B. Lipovšek, K. Jäger, B. Macco, A. Al-Ashouri, J. Krč, L. Korte, B. Rech, R. Schlatmann, M. Topič, B. Stannowski and S. Albrecht, *Energy Environ. Sci.*, 2018, **11**, 3511–3523.
20 J. F. Geisz, R. M. France, K. L. Schulte, M. A. Steiner, A. G. Norman, H. L. Guthrey, M. R. Young, T. Song and T. Moriarty, *Nat. Energy*, 2020, **5**, 326–335.
21 W. Zhang, G. E. Eperon and H. J. Snaith, *Nat. Energy*, 2016, **1**, 16048.
22 A. Swarnkar, A. R. Marshall, E. M. Sanehira, B. D. Chernomordik, D. T. Moore, J. A. Christians, T. Chakrabarti and J. M. Luther, *Science*, 2016, **354**, 92–95.
23 W. J. Yin, T. Shi and Y. Yan, *Adv. Mater.*, 2014, **26**, 4653–4658.
24 K. P. Marshall, M. Walker, R. I. Walton and R. A. Hatton, *Nat. Energy*, 2016, **1**, 16178.
25 R. J. Sutton, G. E. Eperon, L. Miranda, E. S. Parrott, B. A. Kamino, J. B. Patel, M. T. Hörantner,

M. B. Johnston, A. A. Haghighirad, D. T. Moore and H. J. Snaith, *Adv. Energy Mater.*, 2016, **6**, 1502458.
26 J. B. Hoffman, A. L. Schleper and P. V. Kamat, *J. Am. Chem. Soc.*, 2016, **138**, 8603–8611.
27 L. Y. Huang and W. R. Lambrecht, *Phys. Rev. B*, 2016, **93**, 195211.
28 Q. A. Akkerman, M. Gandini, F. D. Stasio, P. Rastogi, F. Palazon, G. Bertoni, J. M. Ball, M. Prato, A. Petrozza and L. Manna, *Nat. Energy*, 2016, **2**, 16194.
29 G. E. Eperon, G. M. Paternò, R. J. Sutton, A. Zampetti, A. A. Haghighirad, F. Cacialli and H. J. Snaith, *J. Mater. Chem.*, 2015, **3**, 19688–19695.
30 T. Krishnamoorthy, H. Ding, C. Yan, W. L. Leong, T. Baikie, Z. Zhang, M. Sherburne, S. Li, M. Asta, N. Mathews and S. G. Mhaisalkar, *J. Mater. Chem.*, 2015, **3**, 23829–23832.
31 P. Ramasamy, D. H. Lim, B. Kim, S. H. Lee, M. S. Lee and J. S. Lee, *Chem. Commun.*, 2016, **52**, 2067–2070.
32 P. Cottingham and R. L. Brutchey, *Chem. Commun.*, 2016, 1–3.
33 D. P. Rai, Sandeep, A. Shankar, A. P. Sakhya, T. P. Sinha, B. Merabet, M. Musa Saad H.-E, R. Khenata, A. Boochani, S. Solaymani and R. K. Thapa, *Mater. Chem. Phys.*, 2017, **186**, 620–626.
34 Sandeep, D. P. Rai, A. Shankar, M. P. Ghimire, R. Khenata and R. K. Thapa, *J. Magn. Magn. Mater.*, 2016, **417**, 313–320.
35 Sandeep, D. P. Rai, A. Shankar, R. Khenata, M. P. Ghimire, R. K. Thapa and S. B. Omran, *Int. J. Mod. Phys. B*, 2016, **30**(12), 1650078.
36 Sandeep, D. P. Rai, A. Shankar, M. P. Ghimire, R. Khenata and R. K. Thapa, *Phys. Scr.*, 2015, **90**, 065803.
37 J. Qiu, Y. Qiu, K. Yan, M. Zhong, C. Mu, H. Yan and S. Yang, *Nanoscale*, 2013, **5**, 3245–3248.
38 L. Lang, J. H. Yang, H. R. Liu, H. J. Xiang and X. G. Gong, *Phys. Lett. A*, 2014, **378**, 290–293.
39 G. Murtaza and I. Ahmad, *Phys. B*, 2011, **406**, 3222–3229.
40 H. Jing, R. Sa and G. Xu, *Chem. Phys. Lett.*, 2019, **732**, 136642.
41 Z. L. Ku, Y. G. Rong, M. Xu, T. F. Liu and H. W. Han, *Sci. Rep.*, 2013, **3**, 3132.
42 H. S. Kim, C. R. Lee, J. H. Im, K. B. Lee, T. Moehl, A. Marchioro, S. J. Moon, R. Humphry-Baker, J. H. Yum, J. E. Moser, M. Grätzel and N. G. Park, *Sci. Rep.*, 2012, **2**, 591.
43 H. J. Snaith, *J. Phys. Chem. Lett.*, 2013, **4**, 3623–3630.
44 C. Katan, N. Mercier and J. Even, *Chem. Rev.*, 2019, **119**, 3140–3192.
45 Z. K. Tan, R. S. Moghaddam, M. L. Lai, P. Docampo, R. Higler, F. Deschler, M. Price, A. Sadhanala, L. M. Pazos, D. Credgington, F. Hanusch, T. Bein, H. J. Snaith and R. H. Friend, *Nat. Nanotechnol.*, 2014, **9**, 46.
46 M. A. Fadla, B. Bentria, T. Dahame and A. Benghia, *Phys. B*, 2020, **585**, 412118.
47 M. Baranowski, P. Plochocka, R. Su, L. Legrand, T. Barisien, F. Bernardot, Q. Xiong, C. Testelin and M. Chamarro, *Photonics Res.*, 2020, **8**, A50–A55.
48 G. Morello, M. De Giorgi, S. Kudera, L. Manna, R. Cingolani and M. Anni, *J. Phys. Chem. C*, 2007, **111**, 5846–5849.
49 N. Pandey, A. Kumar and S. Chakrabarti, *RSC Adv.*, 2019, **9**, 29556.
50 L. Protesescu, S. Yakunin, M. Bodnarchuk and F. Krieg, *Nano Lett.*, 2015, **15**, 3692–3696.
51 Y. Xu, Q. Chen, C. Zhang, R. Wang, H. Wu, X. Zhang, G. Xing, W. W. Yu, X. Wang, Y. Zhang and M. Xiao, *J. Am. Chem. Soc.*, 2016, **138**, 3761–3768.
52 Z. K. Tan, R. S. Moghaddam, M. L. Lai, P. Docampo, R. Higler, F. Deschler, M. Price, A. Sadhanala, L. M. Lazos, D. Credgington, F. Hanusch, T. Bein, H. J. Snaith and R. H. Friend, *Nat. Nanotechnol.*, 2014, **9**, 687–692.
53 H. Zhu, Y. Fu, F. Meng, X. Wu, Z. Gong, Q. Ding, M. V. Gustafsson, M. T. Trinh, S. Jin and X. Y. Zhu, *Nat. Mater.*, 2015, **14**, 636–642.
54 J. Deng, J. Li, Z. Yang and M. Wang, *J. Mater. Chem. C*, 2019, **7**, 12415–12440.
55 C. C. Stoumpos, C. D. Malliakas, J. A. Peters, Z. Liu, M. Sebastian, J. Im, T. C. Chasapis, A. C. Wibowo, D. Y. Chung, A. J. Freeman, *et al.*, *Cryst. Growth Des.*, 2013, **13**, 2722–2727.
56 X. Li, Y. Tan, H. Lai, S. Li, Y. Chen, S. Li, P. Xu and J. Yang, *ACS Appl. Mater. Interfaces*, 2019, **11**, 29746–29752.
57 H. Zhang, X. Liu, J. Dong, H. Yu, C. Zhou, B. Zhang, Y. Xu and W. Jie, *Cryst. Growth Des.*, 2017, **17**, 6426–6431.
58 D. N. Dirin, I. Cherniukh, S. Yakunin, Y. Shynkarenko and M. V. Kovalenko, *Chem. Mater.*, 2016, **28**, 8470–8474.
59 P. Ramasamy, D. H. Lim, B. Kim, S. H. Lee, M. S. Lee and J. S. Lee, *Chem. Commun.*, 2016, **52**, 2067–2070.
60 Y. Lee, J. Kwon, E. Hwang, C. H. Ra, W. J. Yoo, J. H. Ahn, J. H. Park and J. H. Cho, *Adv. Mater.*, 2015, **27**, 41–46.
61 Y. Wang, Y. Zhang, Y. Lu, W. Xu, H. Mu, C. Chen, H. Qiao, J. Song, S. Li, B. Sun, Y. B. Cheng and Q. Bao, *Adv. Opt. Mater.*, 2015, **3**, 1389–1396.
62 W. Y. Nie, H. H. Tsai, R. Asadpour, J. C. Blancon, A. J. Neukirch, G. Gupta, J. J. Crochet, M. Chhowalla, S. Tretiak, M. A. Alam, H. L. Wang and A. D. Mohite, *Science*, 2015, **347**, 522–525.
63 M. A. Green, A. Ho-Baillie and H. J. Snaith, *Nat. Photonics*, 2014, **8**, 506–514.
64 G. Xing, N. Mathews, S. Sun, S. S. Lim, Y. M. Lam, M. Gratzel, S. Mhaisalkar and T. C. Sum, *Science*, 2013, **342**, 344–347.
65 X. Li, F. Cao, D. Yu, J. Chen, Z. Sun, Y. Shen, Y. Zhu, L. Wang, Y. Wei, Y. Wu and H. Zeng, *Small*, 2017, **13**, 1603996.
66 X. Li, Y. Liu, X. Song, H. Wang, H. Gu and H. Zeng, *Angew. Chem., Int. Ed. Engl.*, 2015, **54**, 1759–1764.
67 J. Song, J. Li, X. Li, L. Xu, Y. Dong and H. Zeng, *Adv. Mater.*, 2015, **27**, 7162–7167.
68 J. Li, L. Xu, T. Wang, J. Song, J. Chen, J. Xue, Y. Dong, B. Cai, Q. Shan, B. Han and H. Zeng, *Adv. Mater.*, 2017, **29**, 1603885.
69 K. Lin, J. Xing, L. N. Quan, F. P. G. de Arquer, X. Gong, J. Lu, L. Xie, W. Zhao, D. Zhang, C. Yan, W. Li, X. Liu, Y. Lu, J. Kirman, E. H. Sargent, Q. Xiong and Z. Wei, *Nature*, 2018, **562**, 245–248.

70 Y. Wang, X. Li, J. Song, L. Xiao, H. Zeng and H. Sun, *Adv. Mater.*, 2015, **27**, 7101–7108.
71 Q. Zhang, R. Su, W. Du, X. Liu, L. Zhao, S. T. Ha and Q. Xiong, *Small Methods*, 2017, **1**, 1700163.
72 R. Su, C. Diederichs, J. Wang, T. C. H. Liew, J. Zhao, S. Liu, W. Xu, Z. Chen and Q. Xiong, *Nano Lett.*, 2017, **17**, 3982–3988.
73 R. J. Sutton, G. E. Eperon, L. Miranda, E. S. Parrott, B. A. Kamino, J. B. Patel, M. T. Hörantner, M. B. Johnston, A. A. Haghighirad, D. T. Moore and H. J. Snaith, *Adv. Energy Mater.*, 2016, **6**, 1502458.
74 E. M. Senehira, A. R. Marshall, J. A. Christians, S. P. Harvey, P. N. Ciesielski, L. M. Wheeler, P. Schulz, L. Y. Lin, M. C. Beard and J. M. Luther, *Sci. Adv.*, 2017, **3**, 4204.
75 P. Ramasamy, D. M. Lim, B. Kim, S. H. Lee, M. S. Lee and J. S. Lee, *Chem. Commun.*, 2016, **52**, 2067–2070.
76 S. Wang, K. Wang, Z. Gu, Y. Wang, C. Huang, N. Yi, S. Xiao and Q. Song, *Adv. Opt. Mater.*, 2017, **5**, 1700023.
77 H. M. Ghaithan, Z. A. Alahmed, S. M. H. Qaid, M. Hezam and A. S. Aldwayyan, *ACS Omega*, 2020, **5**, 7468–7480.
78 T. G. Liashenko, E. D. Cherotchenko, A. P. Pushkarev, V. Pakštas, A. Naujokaitis, S. A. Khubezhov, R. G. Polozkov, K. B. Agapev, A. A. Zakhidov, I. A. Shelykh and S. V. Makarov, *Phys. Chem. Chem. Phys.*, 2019, **21**, 18930–18938.
79 S. Plesko, R. Kind and J. Roos, *J. Phys. Soc. Jpn.*, 1978, **45**, 553–557.
80 F. Zhang, H. Zhong, C. Chen, X. Wu, X. Hu, H. Huang, J. Han, B. Zou and Y. Dong, *ACS Nano*, 2015, **9**, 4533.
81 L. Protesescu, S. Yakunin, M. I. Bodnarchuk, F. Krieg, R. Caputo, C. H. Hendon, R. X. Yang, A. Walsh and M. V. Kovalenko, *Nano Lett.*, 2015, **15**, 3692.
82 O. Yu. Posudievsky, N. V. Konoshchuk, V. L. Karbivskyy, O. P. Boiko, V. G. Koshechko and V. D. Pokhodenk, *Theor. Exp. Chem.*, 2017, **53**, 235–243.
83 G. E. Eperon, G. M. Paterno, R. J. Sutton, A. Zampetti, A. A. Haghighirad, F. Cacialli and H. J. Snaith, *J. Mater. Chem. A*, 2015, **3**, 19688–19695.
84 J. A. Steele, H. Jin, I. Dovgaliuk, R. F. Berger, T. Braeckevelt, H. Yuan, C. Martin, E. Solano, K. Lejaeghere, S. M. J. Rogge, C. Notebaert, W. Vandezande, K. P. F. Janssen, B. Goderis, E. Debroye, Y. K. Wang, Y. Dong, D. Ma, M. Saidaminov, H. Tan, Z. Lu, V. Dyadkin, D. Chernyshov, V. V. Speybroeck, E. H. Sargent, J. Hofkens and M. B. J. Roeffaers, *Science*, 2019, **365**, 679.
85 J. B. Hoffman, A. L. Schleper and P. V. Kamat, *J. Am. Chem. Soc.*, 2016, **138**, 8603–8611.
86 S. De Wolf, J. Holovsky, S. J. in Moon, P. Löper, B. Niesen, M. Ledinsky, F. J. Haug, J. H. Yum and C. Ballif, *J. Phys. Chem. Lett.*, 2014, **5**, 1035–1039.
87 G. Liu, L. Kong, W. Yang and H.-k. Mao, *Mater. Today*, 2019, **27**, 91.
88 M. Coduri, T. B. Shiell, T. A. Strobel, A. Mahata, F. Cova, E. Mosconi, F. De Angelis and L. Malavasi, *Mater. Adv.*, 2020, **1**, 2840.
89 M. I. Kholil and M. T. H. Bhuiyan, *J. Phys. Chem. Solids*, 2021, **154**, 110083.
90 Y. Li, J. Liu, P. Zhang, J. Zhang, N. Xiao, L. Yu and P. Niu, *J. Mater. Sci.*, 2020, **55**, 14873.
91 J.-H. Lee, A. Jaffe, Y. Lin, H. I. Karunadasa and J. B. Neaton, *ACS Energy Lett.*, 2020, **5**, 2174.
92 O. V. Oyelade, O. K. Oyewole, D. O. Oyewole, S. A. Adeniji, R. Ichwani, D. M. Sanni and W. O. Soboyejo, *Sci. Rep.*, 2020, **10**, 7183.
93 S. Yalameha, P. Saeidi, Z. Nourbakhsh and A. V. A. Ramazani, *J. Appl. Phys.*, 2020, **127**, 085102.
94 R. Y. Alyoubi, B. M. Raffah, F. Hamioud and A. A. Mubarak, *Mod. Phys. Lett. B*, 2021, **35**, 2150056.
95 S. Idrissi, H. Labrim, S. Ziti and L. Bahmad, *J. Appl. Phys.*, 2020, **126**(3), 190.
96 S. Idrissi, H. Labrim, S. Ziti and L. Bahmad, *Phys. Lett. A*, 2020, **384**, 126453.
97 S. Idrissi, H. Labrim, S. Ziti and L. Bahmad, *J. Supercond. Novel Magn.*, 2020, **33**, 3087–3095.
98 P. Hohenberg and W. Kohn, *Phys. Rev. B*, 1964, **136**, 864.
99 W. Kohn and L. J. Sham, *Phys. Rev. A*, 1965, **140**, 1133.
100 S. J. Clark, M. D. Segall, C. J. Pickard, P. J. Hasnip, M. I. Probert, K. Refson and M. C. Payne, *Z. Kristallogr.*, 2005, **220**, 567.
101 J. Hutton, R. J. Nelmes, G. M. Meyer and V. R. Eiriksson, *J. Phys. C Solid State Phys.*, 1979, **12**, 5393–5410.
102 M. Ahmad, G. Rehman, L. Ali, M. Shafiq, R. Iqbal, R. Ahmad, T. Khan, S. Jalali-Asadabadi, M. Maqbool and I. Ahmad, *J. Alloys Compd.*, 2017, **705**, 828–839.
103 M. Roknuzzaman, K. Ostrikov, H. Wang, A. Du and T. Tesfamichael, *Sci. Rep.*, 2017, **7**, 14025.
104 S. Idrissi a, S. Ziti b, H. Labrim c and L. Bahmad, *Mater. Sci. Semicond. Process.*, 2021, **122**, 105484.
105 M. A. Ghebouli, B. Ghebouli and M. Fatmi, *Phys. B*, 2011, **406**, 1837–1843.
106 A. Najim, B. Hartiti, H. Absike, H. J. T. Nkuissi, H. Labrim, S. Fadili, P. Thevenin and M. Ertugrul, *Mater. Sci. Semicond. Process.*, 2022, **141**, 106442.
107 H. Joshi, R. K. Thapa, A. Laref, W. Sukkabot, L. Pachuau, L. Vanchhawng, P. Grima-Gallardofgh, M. Musa Saad H-E and D. P. Rai, *Surf. Interfaces*, 2022, **30**, 101829.
108 Z. Zhao, M. Zhong, W. Zhou, Y. Peng, Y. Yin, D. Tang and B. Zou, *J. Phys. Chem. C*, 2019, **123**, 25349–25358.
109 L. K. Gao and Y. L. Tang, Theoretical Study on the Carrier Mobility and Optical Properties of CsPbI3 by DFT, *ACS Omega*, 2021, **6**(17), 11545–11555.
110 D. M. Trots and S. V. Myagkota, *J. Phys. Chem. Solids*, 2008, **69**, 2520–2526.
111 M. Born, *Math. Proc. Cambridge Philos. Soc.*, 1940, **36**, 160.
112 J. M. J. den Toonder, J. A. W. van Dommelen and F. P. T. Baaijens, *Modell. Simul. Mater. Sci. Eng.*, 1999, **7**, 909.
113 M. H. K. Rubel, M. A. Hadi, M. M. Rahaman, M. S. Ali, M. Aftabuzzaman, R. Parvin, A. K. M. A. Islam and N. Kumada, *Comput. Mater. Sci.*, 2017, **138**, 160.
114 M. Roknuzzaman, M. A. Hadi, M. A. Ali, M. M. Hossain, N. Jahan, M. M. Uddin, J. A. Alarco and K. Ostrikov, *J. Alloys Compd.*, 2017, **727**, 616.

115 M. A. Hadi, M. N. Islam and M. H. Babu, *Z. Naturforsch.*, 2019, **74**, 71–81.
116 D. G. Pettifor, *Mater. Sci. Technol.*, 1992, **8**, 345.
117 S. F. Pugh, *Philos. Mag.*, 1954, **45**, 823.
118 M. E. Fine, L. D. Brown and H. L. Marcus, *Scr. Metall.*, 1984, **18**, 951.
119 T. Paul, B. K. Chatterjee, S. Maiti, S. Sarkar, N. Besra, B. K. Das, K. J. Panigrahi, S. Thakur1, U. K. Ghorai and K. K. Chattopadhyay, *J. Mater. Chem. C*, 2018, **6**, 3322–3333.
120 G. E. Eperon, S. D. Stranks, C. Menelaou, M. B. Johnston, L. M. Herz and H. J. Snaith, *Energy Environ. Sci.*, 2014, **7**, 982–988.
121 Li Lang, Y.-Yu Zhang, P. Xu, S. Chen, H. J. Xiang and X. G. Gong, *Phys. Rev. B*, 2015, **92**, 075102.
122 K. Heidrich, W. Schafer, M. Schreiber, J. Sochtig, G. Trendel and J. Treusch, *Phys. Rev. B: Condens. Matter*, 1981, **24**, 5642.
123 R. L. Moreira and A. Dias, *J. Phys. Chem. Solids*, 2007, **68**, 1617.
124 J. Islam and A. K. M. A. Hossain, *Sci. Rep.*, 2020, **10**, 14542.
125 X. Liu, B. Xie, C. Duan, Z. Wang, B. Fan, K. Zhang, B. Lin, F. J. M. Colberts, W. Ma, R. A. J. Janssen, F. Huang and Y. Cao, *J. Mater. Chem. A*, 2018, **6**, 395.
126 S. Saha, T. P. Sinha and A. Mookerjee, *Phys. Rev. B*, 2000, **62**, 8828.
127 M. I. Kholil, M. T. H. Bhuiyan, M. A. Rahman, M. S. Ali and M. Aftabuzzaman, *RSC Adv.*, 2021, **11**, 2405.
128 Y. Saeed, B. Amin, H. Khalil, F. Rehman, H. Ali, M. I. Khan, A. Mahmood and M. Shafiq, *RSC Adv.*, 2020, **10**, 17444.
129 Y. Gong, H. Yu and X. Quan, *Int. J. Photoenergy*, 2014, **2014**, 5.
130 J. Liu, S. Chen, Q. Liu, Y. Zhu and J. Zhang, *Chem. Phys. Lett.*, 2013, **572**, 101–105.